Article

On the Choice of Interface Parameters in Robin–Robin Loosely Coupled Schemes for Fluid–Structure Interaction

Giacomo Gigante [1] and Christian Vergara [2],*

1   Dipartimento di Ingegneria Gestionale, dell'Informazione e della Produzione,
    Università degli Studi di Bergamo, 24044 Dalmine, Italy; giacomo.gigante@unibg.it
2   LABS, Dipartimento di Chimica, Materiali e Ingegneria Chimica "Giulio Natta", Politecnico di Milano,
    20133 Milan, Italy
*   Correspondence: christian.vergara@polimi.it

Abstract: We consider two loosely coupled schemes for the solution of the fluid–structure interaction problem in the presence of large added mass effect. In particular, we introduce the Robin–Robin and Robin–Neumann explicit schemes where suitable interface conditions of Robin type are used. For the estimate of interface Robin parameters which guarantee stability of the numerical solution, we propose a new strategy based on the optimization of the reduction factor of the corresponding strongly coupled (implicit) scheme, by means of the optimized Schwarz method. To check the suitability of our proposals, we show numerical results both in an ideal cylindrical domain and in a real human carotid. Our results showed the effectiveness of our proposal for the calibration of interface parameters, which leads to stable results and shows how the explicit solution tends to the implicit one for decreasing values of the time discretization parameter.

1. Introduction

The numerical solution of fluid–structure interaction (FSI) problems is very challenging and many different strategies have been considered so far. Among them, we mention monolithic strategies where the whole space and time discretized problem (e.g., due to Finite Elements) is solved by means of efficient linear solvers and ad-hoc preconditioners that should accelerate convergence which in general is quite problematic due to the elevated condition number of the FSI problem, see e.g., [1–6]. Another family of strategies relies on partitioned or segregated schemes which introduce the separate solution of the fluid and structure (and possibly fluid geometry) subproblems. Among them, strongly coupled or implicit strategies solve such problems until convergence of the interface conditions at each time step, see, e.g., [7–16].

Within partitioned schemes, loosely coupled or explicit schemes for the numerical solution of the FSI problem are based on an overall explicit time discretization which leads to the solution of just one fluid and one structure problem per time step. This makes this family of methods very attractive from the computational and implementation point of view and for these reasons they have been widely used in many engineering applications such as aeroelasticity [17–19]. However, loosely coupled schemes suffer from a lack of stability when the added mass effect is relevant (i.e., when the densities of fluid and structure are comparable). This happens, for example, in hemodynamics [20]. In this respect, it is known that the explicit Dirichlet–Neumann (DN) scheme is unconditionally unstable in the hemodynamic regime, see [7,11,21].

Recently, some studies introduced loosely coupled schemes for the FSI problem based on Robin interface conditions, obtained by considering linear combinations of the no-slip condition and action–reaction principle by means of suitable parameters [13,15,22–28].

In such works different proposals for the interface parameters were addressed with the aim of improving the stability properties when the added mass effect is relevant with respect to the explicit DN scheme. In our recent study [29], we have provided for a model problem a stability analysis of the explicit Robin–Neumann (RN) scheme. In particular, we have found sufficient conditions for the interface Robin parameter, guaranteeing both unconditional instability and conditional stability.

In this paper, we address the issue of selecting suitable and easily computable interface parameters both for the explicit RN and the explicit Robin–Robin (RR) schemes, able to guarantee the stability of such loosely coupled schemes. In particular, we discuss the case of cylindrical-like geometries as happens, for example, in vascular hemodynamics and we propose a new and effective way to select such parameters. We start from the analysis based on the optimized Schwarz method [30] provided for the implicit (i.e., strongly coupled) RR scheme in the FSI context in [31]. This allowed us to determine effective values for the Robin interface parameters which guarantee excellent converge property even in presence of large added mass effect (for strongly coupled scheme, a large added mass effect yields a very slow convergence [7]). Here we provide also a new way to easily estimate an effective Robin interface parameter for the RN strongly coupled scheme. The idea of the present work is to use such estimates in the corresponding loosely coupled RN and RR schemes. In particular, we verify the stability of the corresponding numerical solution in 3D FSI numerical experiments.

2. Mathematical and Numerical Setting

2.1. The Continuous Problem

We consider the coupling between the Navier–Stokes equations for an incompressible fluid solved in the Arbitrary Lagrangian-Eulerian (ALE) formulation [32] and the linear infinitesimal elasticity [33]. Let Ω_f and Ω_s be the fluid and structure domains, Σ the fluid–structure interface, Σ^{out} the external structure surface, $\boldsymbol{n} = \boldsymbol{n}_f$ the unit normal outgoing the fluid domain, and $\boldsymbol{n}_s$ the unit normal outgoing the structure domain. We have for each t [33]:

$$\rho_f \partial_t^A \boldsymbol{u} + \rho_f((\boldsymbol{u} - \boldsymbol{\omega}) \cdot \nabla)\boldsymbol{u} - \nabla \cdot \boldsymbol{T}_f(\boldsymbol{u}, p) = \boldsymbol{0} \qquad \text{in } \Omega_f, \qquad (1a)$$

$$\nabla \cdot \boldsymbol{u} = 0 \qquad \text{in } \Omega_f, \qquad (1b)$$

$$\boldsymbol{u} = \partial_t \boldsymbol{\eta} \qquad \text{on } \Sigma, \qquad (1c)$$

$$\boldsymbol{T}_f \boldsymbol{n} = \boldsymbol{T}_s \boldsymbol{n} \qquad \text{on } \Sigma, \qquad (1d)$$

$$\rho_s \partial_{tt} \widehat{\boldsymbol{\eta}} - \nabla \cdot \widehat{\boldsymbol{T}}_s(\widehat{\boldsymbol{\eta}}) = \boldsymbol{0} \qquad \text{in } \widehat{\Omega}_s, \qquad (1e)$$

$$\gamma_{ST} \widehat{\boldsymbol{\eta}} + \widehat{\boldsymbol{T}}_s(\widehat{\boldsymbol{\eta}}) \boldsymbol{n}_s = 0 \qquad \text{on } \widehat{\Sigma}^{out}, \qquad (1f)$$

where $\boldsymbol{T}_f(\boldsymbol{u}, p) = -p\boldsymbol{I} + \mu(\nabla \boldsymbol{u} + (\nabla \boldsymbol{u})^T)$ is the Cauchy stress tensor for the fluid and with μ the dynamic viscosity. ∂_t^A represents the ALE time derivative, i.e., with respect to the ALE framework, and $\boldsymbol{\omega}$ is the velocity of the fluid domain obtained by solving an harmonic extension of the interface velocity with homogeneous Dirichlet or Neumann boundary conditions on $\partial \Omega_f \setminus \Sigma$. Notice that, accordingly, Ω_f changes in time. Instead, the structure problem (1e) is solved in a Lagrangian framework and for this reason we have indicated with $\widehat{\ }$ the corresponding quantities. For the sake of notation, in what follows $\widehat{\ }$ will be understood. Moreover, $\boldsymbol{T}_s$ is the structure Cauchy stress tensor given by

$$\boldsymbol{T}_s(\boldsymbol{\eta}) = \lambda_1(\nabla \boldsymbol{\eta} + (\nabla \boldsymbol{\eta})^T) + \lambda_2(\nabla \cdot \boldsymbol{\eta})\boldsymbol{I},$$

where λ_1 and λ_2 are the Lamé constants that can be defined in terms of the Young modulus E and the Poisson ratio ν as follows

$$\lambda_1 = \frac{E}{2(1 + \nu)}, \quad \lambda_2 = \frac{\nu E}{(1 + \nu)(1 - 2\nu)}.$$

Finally, we observe that condition (1f) represents a Robin condition at the external surface to account for the effect of an elastic surrounding tissue with elasticity modulus γ_{ST} [34]. The previous problem needs to be completed with other boundary conditions and initial conditions for both fluid and structure. Examples of applications where the FSI problem (1) has been considered are hemodynamics, where blood interacts with the vascular wall [33], the respiratory system [35], and aeroelasticity for the study of airfoils [17].

2.2. Robin Robin Loosely Coupled Scheme

In order to write a suitable algorithm for the numerical solution of the FSI problem (1), we consider the following linear combinations of the interface conditions (1c)–(1d), for given scalars $\alpha_f \neq \alpha_s$:

$$\alpha_f \boldsymbol{u} + \boldsymbol{T}_f \boldsymbol{n} = \alpha_f \partial_t \boldsymbol{\eta} + \boldsymbol{T}_s \boldsymbol{n}, \tag{2a}$$

$$\alpha_s \partial_t \boldsymbol{\eta} + \boldsymbol{T}_s \boldsymbol{n} = \alpha_s \boldsymbol{u} + \boldsymbol{T}_f \boldsymbol{n}. \tag{2b}$$

The coupled FSI problem (1) where (1c)–(1d) are substituted by (2a)–(2b) is still equivalent to (1), thus we can introduce suitable numerical strategies based on the exchange of conditions (2a)–(2b). To this aim, we first need to detail the time discretizaton and how we manage the geometric coupling, i.e., the fact that the fluid domain movement depends on the structure displacement. Regarding the time discretization, we used a first order implicit method for both fluid and structure, with a semi-implicit treatment of the fluid convective term, relying on a CFL-like bound for the time discretization Δt. We also consider an explicit treatment of the no-slip condition, allowing in fact to split the two subproblems. Regarding the geometric coupling, it has been shown that in the hemodynamic regime an explicit treatment is enough to provide stable and accurate results [12,14,22,36,37]. This means that the harmonic extension problem for the fluid domain displacement and velocity is solved with structure data that comes from previous time steps. This in fact decouples the geometric and FSI problems, thus at each time step the time discretization of problem (1b)–(1c) is in fact solved in a known domain Ω_f.

Let $t^n = n\Delta t$, $n = 0, \ldots,$ the discrete time instants and $v^n \simeq v(t^n)$ the approximation at time t^n of a function of time $v(t)$. Thus, for the numerical solution of problem (1b), (1c), (2a), (2b), (1e), and (1f), we introduce in Algorithm 1 the Explicit Robin–Robin loosely coupled scheme, obtained after time discretization and by prescribing condition (2a) as boundary condition for the fluid problem, with structure quantities taken from the previous time step, and condition (2b) to the structure problem.

Remark 1. *As observed, at the continuous level conditions* (2a) *and* (2b) *are perfectly equivalent to* (1c) *and* (1d)*. After the numerical discretization and the selection of an explicit treatment, we obtain conditions* (3c) *and* (4b) *which satisfy the original interface conditions up to an error of the order of* Δt.

Remark 2. *The implicit (strongly coupled) Robin–Robin scheme is obtained from Algorithm 1 by replacing the right hand side of* (3c) *with* $\alpha_f \frac{\boldsymbol{\eta}^{n+1} - \boldsymbol{\eta}^n}{\Delta t} + \boldsymbol{T}_s(\boldsymbol{\eta}^{n+1})$ *and then subiterating with the structure problem* (4).

Algorithm 1 Explicit Robin–Robin scheme

Given two scalars $\alpha_f \neq \alpha_s$ and quantities at previous time steps, at time step t^{n+1} solve in sequence:

1: A fluid problem with a Robin condition at the fluid–structure interface:

$$\rho_f \frac{\boldsymbol{u}^{n+1} - \boldsymbol{u}^n}{\Delta t} + \rho_f((\boldsymbol{u}^n - \boldsymbol{\omega}^n) \cdot \nabla)\boldsymbol{u}^{n+1} - \nabla \cdot \boldsymbol{T}_f(\boldsymbol{u}^{n+1}, p^{n+1}) = \boldsymbol{0} \qquad \text{in } \Omega_f^n, \quad (3a)$$

$$\nabla \cdot \boldsymbol{u}^{n+1} = 0 \qquad \text{in } \Omega_f^n, \quad (3b)$$

$$\alpha_f \boldsymbol{u}^{n+1} + \boldsymbol{T}_f(\boldsymbol{u}^{n+1}, p^{n+1})\boldsymbol{n} = \alpha_f \frac{\boldsymbol{\eta}^n - \boldsymbol{\eta}^{n-1}}{\Delta t} + \boldsymbol{T}_s(\boldsymbol{\eta}^n) \qquad \text{on } \Sigma^n; \quad (3c)$$

2: A structure problem with a Robin condition at the fluid–structure interface:

$$\rho_s \frac{\boldsymbol{\eta}^{n+1} - 2\boldsymbol{\eta}^n + \boldsymbol{\eta}^{n-1}}{\Delta t^2} - \nabla \cdot \boldsymbol{T}_s(\boldsymbol{\eta}^{n+1}) = \boldsymbol{0} \qquad \text{in } \Omega_s^0, \quad (4a)$$

$$\alpha_s \boldsymbol{\eta}^{n+1} + \Delta t \boldsymbol{T}_s(\boldsymbol{\eta}^{n+1}) = \alpha_s \Delta t \boldsymbol{u}^{n+1} + \Delta t \boldsymbol{T}_f(\boldsymbol{u}^{n+1}, p^{n+1})\boldsymbol{n} + \alpha_s \boldsymbol{\eta}^n \qquad \text{on } \Sigma^0, \quad (4b)$$

$$\gamma_{ST} \boldsymbol{\eta}^{n+1} + \boldsymbol{T}_s(\boldsymbol{\eta}^{n+1})\boldsymbol{n}_s = 0 \qquad \text{on } \Sigma^{out}. \quad (4c)$$

In what follows we discuss the choice of the interface parameters α_f and α_s in the case of cylindrical-like geometries and interface, a situation which occurs in many applications with large added mass effect, e.g., in hemodynamics.

3. On the Choice of the Interface Parameters

3.1. Convergence Analysis of the Implicit Robin–Robin Scheme

Our starting point is the optimization procedure to properly select the interface parameters in the implicit Robin–Robin scheme for a simplified FSI problem in the case of cylindrical geometries in [31], whose main results are here reviewed for the sake of completeness.

We consider the problem arising from the interaction between an incompressible, inviscid, and linear fluid occupying the fixed domain $\Omega_f = \{(x_1, x_2, y) \in \mathbb{R}^3 : x_1^2 + x_2^2 < R^2\}$, and a linear elastic structure modeled with the wave equation occupying the domain $\Omega_s = \{(x_1, x_2, y) \in \mathbb{R}^3 : R^2 < x_1^2 + x_2^2 < (R + H)^2\}$, where $\Sigma_{out} = \{(x_1, x_2, y) \in \mathbb{R}^3 : x_1^2 + x_2^2 = (R + H)^2\}$ is the external surface. The two subproblems interact at the interface $\Sigma = \{(x_1, x_2, y) \in \mathbb{R}^3 : x_1^2 + x_2^2 = R^2\}$. In Algorithm 2 we report the implicit Robin–Robin scheme at time t^{n+1} for the solution of this simplified FSI problem. Actual temporal index $n + 1$ is understood. Notice that the coupling occurs only in the radial direction r since the fluid is inviscid. We have indicated with u_r and η_r the radial fluid velocity and structure displacement, respectively, and with F_1 and F_2 terms coming from the previous time step.

Notice that in [31] we considered general operators $\mathcal{S}_f$ and $\mathcal{S}_s$ to build the interface linear combinations. Here for the sake of exposition, we limit ourselves to the scalar constant case since the forthcoming optimization is performed over the subset of the scalars.

Algorithm 2 Implicit Robin–Robin scheme for the simplified FSI problem

---

Given two scalars $\alpha_f \neq \alpha_s$ and quantities at previous time steps, solve for $k \geq 1$ until convergence:

1: A fluid problem with a Robin condition at the fluid–structure interface:

$$\rho_f \frac{\boldsymbol{u}^{(k)} - \boldsymbol{u}^n}{\Delta t} + \nabla p^{(k)} = \boldsymbol{0} \qquad \text{in } \Omega_f,$$

$$\nabla \cdot \boldsymbol{u}^{(k)} = 0 \qquad \text{in } \Omega_f,$$

$$\alpha_f u_r^{(k)} - p^{(k)} = \alpha_f \frac{\eta_r^{(k-1)}}{\Delta t} + \lambda \frac{\partial \eta_r^{(k-1)}}{\partial \boldsymbol{n}} + F_1(u_r^n, \eta_r^n) \qquad \text{on } \Sigma;$$

2: A structure (wave) problem with a Robin condition at the fluid–structure interface:

$$\rho_s \frac{\boldsymbol{\eta}^{(k)} - 2\boldsymbol{\eta}^n + \boldsymbol{\eta}^{n-1}}{\Delta t^2} - \lambda \triangle \boldsymbol{\eta}^{(k)} = \boldsymbol{0} \qquad \text{in } \Omega_s,$$

$$\alpha_s \eta_r^{(k)} + \Delta t \lambda \frac{\partial \eta_r^{(k)}}{\partial \boldsymbol{n}} = \alpha_s \Delta t u_r^{(k)} - \Delta t p^{(k)} + F_2(u_r^n, \eta_r^n) \qquad \text{on } \Sigma,$$

$$\boldsymbol{\eta}^{(k)} \times \boldsymbol{n} = \boldsymbol{0} \qquad \text{on } \Sigma,$$

$$\boldsymbol{\eta}^{(k)} \times \boldsymbol{n} = \boldsymbol{0} \qquad \text{on } \Sigma,$$

$$\gamma_{ST} \boldsymbol{\eta}^{(k)} + \lambda \frac{\partial \boldsymbol{\eta}^{(k)}}{\partial \boldsymbol{n}} = \boldsymbol{0} \qquad \text{on } \Sigma^{out}.$$

3.2. Selection of Effective Interface Parameter Values for the Explicit Robin–Robin Scheme

Following [31], set

$$A(m,k) = -\frac{\lambda \Delta t \beta (K'_m(\beta R) - \chi I'_m(\beta R))}{K_m(\beta R) - \chi I_m(\beta R)}, \tag{5a}$$

$$B(m,k) = -\frac{\rho_f I_m(kR)}{\Delta t \, k \, I'_m(kR)}, \tag{5b}$$

$$\beta(k) = \sqrt{k^2 + \frac{\rho_s}{\lambda \Delta t^2}}, \tag{5c}$$

$$\chi(m,k) = \frac{\gamma_{ST} K_m(\beta(R+H)) + \lambda \beta K'_m(\beta(R+H))}{\gamma_{ST} I_m(\beta(R+H)) + \lambda \beta I'_m(\beta(R+H))}, \tag{5d}$$

$$\overline{B} := \max_{(m,k) \in K} B(m,k), \qquad \overline{A} := \min_{(m,k) \in K} A(m,k), \tag{5e}$$

$$\overline{M} = \frac{1}{2}(\overline{A} + \overline{B}), \tag{5f}$$

$$D(m,k) = \frac{1}{2}(A(m,k) - B(m,k)), \qquad M(m,k) = \frac{1}{2}(A(m,k) + B(m,k)), \tag{5g}$$

$$Q(m,k) = \frac{|M(m,k) - \overline{M}|}{D(m,k)}, \quad \overline{Q} = \sup_{(m,k) \in K} Q(m,k), \quad N = \frac{\inf_{(m,k) \in K} D(m,k)}{\sup_{(m,k) \in K} D(m,k)}, \tag{5h}$$

$$\rho_0 = \max \left\{ \left(\frac{1 - \sqrt{N}}{1 + \sqrt{N}}\right)^2 ; \left(\frac{1 - \sqrt{1 - \overline{Q}^2}}{\overline{Q}}\right)^2 \right\}, \tag{5i}$$

where $k \geq 0$ and $m = 0, 1, 2, \ldots$ are the frequencies related to the axial and circumferential coordinates, respectively, and which belong to the set K, I_m and K_m are the modified Bessel

functions [38]. Then, in [31] it has been proven, through the optimized Schwarz method, that the reduction factor related to Algorithm 2 is given by

$$\rho(m,k) = \left| \frac{\alpha_f - A(m,k)}{\alpha_s - A(m,k)} \cdot \frac{\alpha_s - B(m,k)}{\alpha_f - B(m,k)} \right|. \tag{6}$$

In particular, it has been proposed to look for parameter values along the straight line $\alpha_f = p$ and $\alpha_s = -p + 2\overline{M}$ for varying $p \in \mathbb{R}$. With this specific choice, the reduction factor (6) becomes

$$\rho(m,k) = \left| \frac{p - A(m,k)}{2\overline{M} - p - A(m,k)} \frac{2\overline{M} - p - B(m,k)}{p - B(m,k)} \right|, \tag{7}$$

and it has been proved that it satisfies

$$\rho(m,k) \leq \rho_0$$

for any $(m,k) \in K$ if and only if $p \in [p_-, p_+]$ with

$$\begin{aligned}
p_- &= \overline{M} \\
&+ \sup_{(m,k) \in K} \left\{ \frac{1+\rho_0}{1-\rho_0} D(m,k) - \sqrt{\left(\overline{M} - M(m,k)\right)^2 + \frac{4\rho_0}{(1-\rho_0)^2} (D(m,k))^2} \right\}, \\
p_+ &= \overline{M} \\
&+ \inf_{(m,k) \in K} \left\{ \frac{1+\rho_0}{1-\rho_0} D(m,k) + \sqrt{\left(\overline{M} - M(m,k)\right)^2 + \frac{4\rho_0}{(1-\rho_0)^2} (D(m,k))^2} \right\}.
\end{aligned} \tag{8}$$

The previous result provided an easy way to compute a range of values of p (and thus of α_f and α_s) which guarantees convergence for any frequencies $(m,k) \in K$. Moreover, this range contains the optimal value p^* of p which minimizes the reduction factor for the choice $\alpha_f = p$ and $\alpha_s = -p + 2\overline{M}$, which could be easily found manually. The efficiency of such procedure has been shown in [31] both in ideal and in realistic carotid geometries in the context of hemodynamics. An extension to the case of spherical geometries and interfaces has been provided in [39].

The idea proposed in this paper is to use the range $p \in [p_-, p_+]$ given by (8) to properly select the interface parameters in the explicit Robin–Robin Algorithm 1, still with the specific choice $\alpha_f = p$ and $\alpha_s = -p + 2\overline{M}$. In particular, we propose here to use the optimal value p^* also for the explicit RR scheme. Indeed, we expect that the interface Robin parameters that guarantee a fast convergence in the implicit case should guarantee stability and accuracy for the explicit case. Although there is not yet a proof of this, we provide here an experimental analysis to support our choices, see Section 4.

3.3. An Alternative Way to Select the Interface Parameter in the Explicit Robin–Neumann Scheme

We consider now the implicit Robin–Neumann scheme, i.e., Algorithm 2 with $\alpha_s = 0$. We propose here a new way to efficiently select the parameter α_f for this algorithm. In particular, we still look for $\alpha_f = p$ with p a scalar independent of the frequencies.

We have the following result.

Theorem 1. *Suppose to have for a given iterative algorithm a reduction factor of the form*

$$\rho(k) = \left| \frac{p - A(k)}{p - B(k)} \cdot \frac{B(k)}{A(k)} \right|, \tag{9}$$

for suitable scalar functions $A(k)$ and $B(k)$ defined on K, where k is a general scalar or vector variable, and with $A(k)B(k) \neq 0$ for all $k \in K$. Then, by setting

$$a = \frac{1}{A}, \qquad b = \frac{1}{B},$$
$$\overline{a} = \max_{k \in K} a(k), \qquad \underline{a} = \min_{k \in K} a(k),$$
$$\overline{b} = \max_{k \in K} b(k), \qquad \underline{b} = \min_{k \in K} b(k),$$

if $\overline{b} < \underline{a}$, we have

$$\rho(k) \leq \theta = \frac{\overline{a} - \underline{a}}{\overline{a} + \underline{a} - 2\overline{b}} < 1, \tag{10}$$

for any $k \in K$ provided that

$$\frac{1}{p} \in \left[\frac{\max_{k \in K}(a(k) + \theta b(k))}{1 + \theta}, \frac{\min_{k \in K}(a(k) - \theta b(k))}{1 - \theta} \right]. \tag{11}$$

Proof. Notice that for any $\theta \in [0, 1)$ we have

$$\frac{\max_{k \in K}(a(k) + \theta b(k))}{1 + \theta} \leq \frac{\overline{a} + \theta \overline{b}}{1 + \theta}$$

and

$$\frac{\underline{a} - \theta \overline{b}}{1 - \theta} \leq \frac{\min_{k \in K}(a(k) - \theta b(k))}{1 - \theta}.$$

By imposing

$$\frac{\overline{a} + \theta \overline{b}}{1 + \theta} = \frac{\underline{a} - \theta \overline{b}}{1 - \theta},$$

i.e., for

$$\theta = \frac{\overline{a} - \underline{a}}{\overline{a} + \underline{a} - 2\overline{b}} \in [0, 1),$$

we can write

$$\frac{\max_{k \in K}(a(k) + \theta b(k))}{1 + \theta} \leq \frac{\min_{k \in K}(a(k) - \theta b(k))}{1 - \theta}. \tag{12}$$

Now, setting

$$q = \frac{1}{p},$$

we can write the reduction factor (9) as follows

$$\rho(k) = \left| \frac{\frac{1}{q} - \frac{1}{a(k)}}{\frac{1}{q} - \frac{1}{b(k)}} \cdot \frac{\frac{1}{b(k)}}{\frac{1}{a(k)}} \right| = \left| \frac{a(k) - q}{b(k) - q} \right|.$$

One only has to observe now that inequality (10), that is

$$-\theta \leq \frac{a(k) - q}{b(k) - q} \leq \theta$$

is equivalent to

$$\frac{a(k) + \theta b(k)}{1 + \theta} \leq q \leq \frac{a(k) - \theta b(k)}{1 - \theta},$$

which makes sense for any $k \in K$ owing to (12). Thus the thesis follows. $\square$

We can now apply the above result to our case, i.e., the implicit Robin–Neumann scheme (Algorithm 2 with $\alpha_s = 0$), interpreting k in Theorem 1 as the couple of frequencies

(m, k) and by taking A and B as in (5a)–(5d). Indeed, from (6), by setting $\alpha_f = p$ and $\alpha_s = 0$, we obtain

$$\rho(m, k) = \left| \frac{p - A(m, k)}{-A(m, k)} \cdot \frac{-B(m, k)}{p - B(m, k)} \right| = \left| \frac{p - A(m, k)}{p - B(m, k)} \cdot \frac{B(m, k)}{A(m, k)} \right|.$$

We now only need to prove that, as requested by Theorem 1, $\overline{b} < \underline{a}$. To this aim, we prove the following result.

Lemma 1. *For all integers $m \geq 0$ and for all $k \geq 0$, one has*

$$a(m, k) = \frac{1}{A(m, k)} = \frac{K_m(\beta R) - \chi I_m(\beta R)}{\lambda \Delta t \beta (-K'_m(\beta R) + \chi I'_m(\beta R))} > 0$$

and

$$b(m, k) = \frac{1}{B(m, k)} = -\frac{\Delta t k I'_m(|k|R)}{\rho_f I_m(kR)} \leq 0,$$

with β and χ given by (5c) and(5d). When $k = 0$, the expression for $b(m, k)$ has to be intended as $k \to 0$, that is

$$b(m, 0) = -\frac{\Delta t m}{\rho_f R}.$$

Proof. The estimate for $b(m, k)$ is trivial, since both I_m and I'_m are positive functions.

Concerning $a(m, k)$, for notational convenience, set $x = \beta R$, $h = \beta H$, and $c = \lambda \beta / \gamma_{ST}$. The numerator of $a(m, k)$ is positive if and only if

$$\frac{K_m(x)}{I_m(x)} > \chi = \frac{K_m(x + h) + c K'_m(x + h)}{I_m(x + h) + c I'_m(x + h)}.$$

Since K_m / I_m is decreasing on $(0, +\infty)$, it suffices to show that for all $x > 0$,

$$\frac{K_m(x)}{I_m(x)} > \frac{K_m(x) + c K'_m(x)}{I_m(x) + c I'_m(x)},$$

and this follows immediately since $K'_m(x) < 0$ and $I'_m(x) > 0$. Similarly, the denominator of $a(m, k)$ is positive if and only if

$$\frac{-K'_m(x)}{I'_m(x)} > -\chi = \frac{-K_m(x + h) - c K'_m(x + h)}{I_m(x + h) + c I'_m(x + h)}.$$

Since

$$\frac{-K'_m(x)}{I'_m(x)} = \frac{K_{m-1}(x) + K_{m+1}(x)}{I_{m-1}(x) + I_{m+1}(x)}$$

is decreasing in $(0, +\infty)$, it suffices to show that for all $x > 0$,

$$\frac{-K'_m(x)}{I'_m(x)} > \frac{-K_m(x) - c K'_m(x)}{I_m(x) + c I'_m(x)},$$

and this follows immediately since $K_m(x) > 0$ and $I_m(x) > 0$. □

Thus, all hypotheses of Theorem 1 are satisfied by our application. The idea we propose in this paper is to use also for the explicit RN scheme (Algorithm 1 with $\alpha_s = 0$) an optimized value p^* found in the range of convergence of its implicit counterpart (11).

4. Numerical Results

4.1. Generalities

In this section we report numerical results aiming at showing the effectiveness of our proposal for the interface Robin parameters in the explicit RR and RN schemes. In particular, we want to understand if the values of the parameters derived by the simplified FSI problem (see Algorithm 2) work well for the complete three-dimensional FSI problem (1) solved by means of Algorithm 1. The use of simplified FSI models to perform analyses whose results are then used for more complex problems is a standard procedure due to the difficulty in analyzing directly such problems. For example, simplified FSI problems have been used to study the convergence of strongly coupled partitioned procedures, then successfully tested over 3D general problems, in [7,9,16,29,40], and to derive the well-known result about the instability of the explicit Dirichlet–Neumann scheme for large added-mass effect in [7,21].

All the simulations are run in the hemodynamic regime, characterized by a large added mass effect and where the stability of loosely coupled methods is a challenging issue.

We consider problem (1) and for its time discretization we used the BDF schemes of order 1 for both fluid and structure, with a semi-implicit treatment of the fluid convective term. For the space discretization we used $P1bubble - P1$ Finite Elements for the fluid and $P1$ Finite Elements for the structure. The fluid domain at each time step is obtained by extrapolation of the previous time step (semi-implicit approach [12,14,37]). We also used the following data: fluid density $\rho_f = 1\,\text{g/cm}^3$, fluid viscosity $\mu = 0.035\,\text{g/(cm s)}$, structure density $\rho_s = 1.1\,\text{g/cm}^3$, Young modulus $E = 3 \times 10^6\,\text{dyne/cm}^2$, Poisson ratio $\nu = 0.49$.

Notice that to compute $A(m,k)$ given by (5a) which is needed for the calibration of the interface parameters, we need the value of λ in the wave equation representing the structure problem in the simplified FSI problem. To do this, we assumed that the value of λ could be approximated by $G\lambda_1$, with $G = \pi^2/12$ the Timoshenko correction factor.

4.2. Test in the Cylinder—Test I

In the first numerical test (test I), the fluid domain is a cylinder with length $L = 5\,\text{cm}$ and radius $R = 0.5\,\text{cm}$, whereas the structure domain is the external cylindrical crown with thickness $H_s = 0.1\,\text{cm}$. The meshes are composed by 4680 tetrahedra and 1050 vertices for the fluid and 1260 vertices for the structure.

At the inlet we prescribed a Neumann condition

$$\boldsymbol{T}_f(\boldsymbol{u}^{n+1}, p^{n+1})\boldsymbol{n} = -P_{in}\boldsymbol{n}, \tag{13}$$

with the following pressure function

$$P_{in} = \widehat{P}\left(1 - \cos\left(\frac{2\pi t}{0.01}\right)\right) \text{ dyne/cm}^2, \quad t \leq T = 0.04\,\text{s},$$

with absorbing resistance conditions at the outlets [22,41].

If not otherwise specified, we used the following parameters (referred to as "basic"): $\widehat{P} = 500$, $\Delta t = 0.0005\,\text{s}$, $\gamma_{ST} = 1.5 \times 10^6\,\text{dyne/cm}^3$. All the numerical results have been obtained with the parallel Finite Element library LIFEV [42].

We will refer to RR-explicit simulation when using α_f and α_s selected in the range (8) described in Section 3.2, whereas to RN-explicit simulation when using α_f in the range (11) as in Section 3.3 and $\alpha_s = 0$. We reported also the numerical solution obtained by using an implicit method, in particular the Robin–Neumann scheme, with an absolute tolerance of 10^{-7} on the convergence of the interface conditions.

In Table 1 we reported the values of the optimized Robin interface parameters a priori estimated via an empirical procedure. In particular, we take $K = [m_{min}, m_{max}] \times [k_{min}, k_{max}]$ with $m_{min} = 0$ and $m_{max} = 10$, $k_{min} = \pi/L = 0.6$ and $k_{max} = \pi/h = 12.5$ (remember that m and k are the angular and longitudinal frequencies) and we empirically look for p that minimizes $\max_{(m,k)\in K} \rho(m,k)$ when either $\alpha_f = p$, $\alpha_s = 2\overline{M} - p$ and p varies in the range (8) (RR-explicit), or $\alpha_f = p$, $\alpha_s = 0$ and p satisfies (11) (RN-Explicit). Notice from

the analyses reported in Sections 3.2 and 3.3 that any change of Δt and γ_{ST} influences the estimates of the interface parameters, whereas the choice of $\widehat{P}$ does not.

Table 1. Values of the Robin interface parameters used in the loosely coupled schemes ([g/(cm^2 s)]). Test I.

	$\alpha_f - $ **RR-expl**	$\alpha_s - $ **RR-expl**	$\alpha_f - $ **RN-expl**
Basic	1045	−169	1084
$\Delta t = 10^{-3}$	1702	−115	1708
$\Delta t = 2.5 \cdot 10^{-4}$	866	−276	904
$\gamma_{ST} = 3 \cdot 10^5$	1526	−138	1590

In Figure 1 we report the time behavior of the mean pressure at the section located at half of the pipe ($z = 2.5\,\text{cm}$) for different values of Δt. In Figure 2, instead we show the same quantity in the case of an increased Reynolds number ($\widehat{P} = 5000$) for two values of the surrounding tissue parameter ($\gamma_{ST} = 3 \times 10^6\,\text{dyne/cm}^3$ and $\gamma_{ST} = 3 \times 10^6\,\text{dyne/cm}^3$) and for a reduced values of the time step ($\Delta t = 1.25 \times 10^{-4}$).
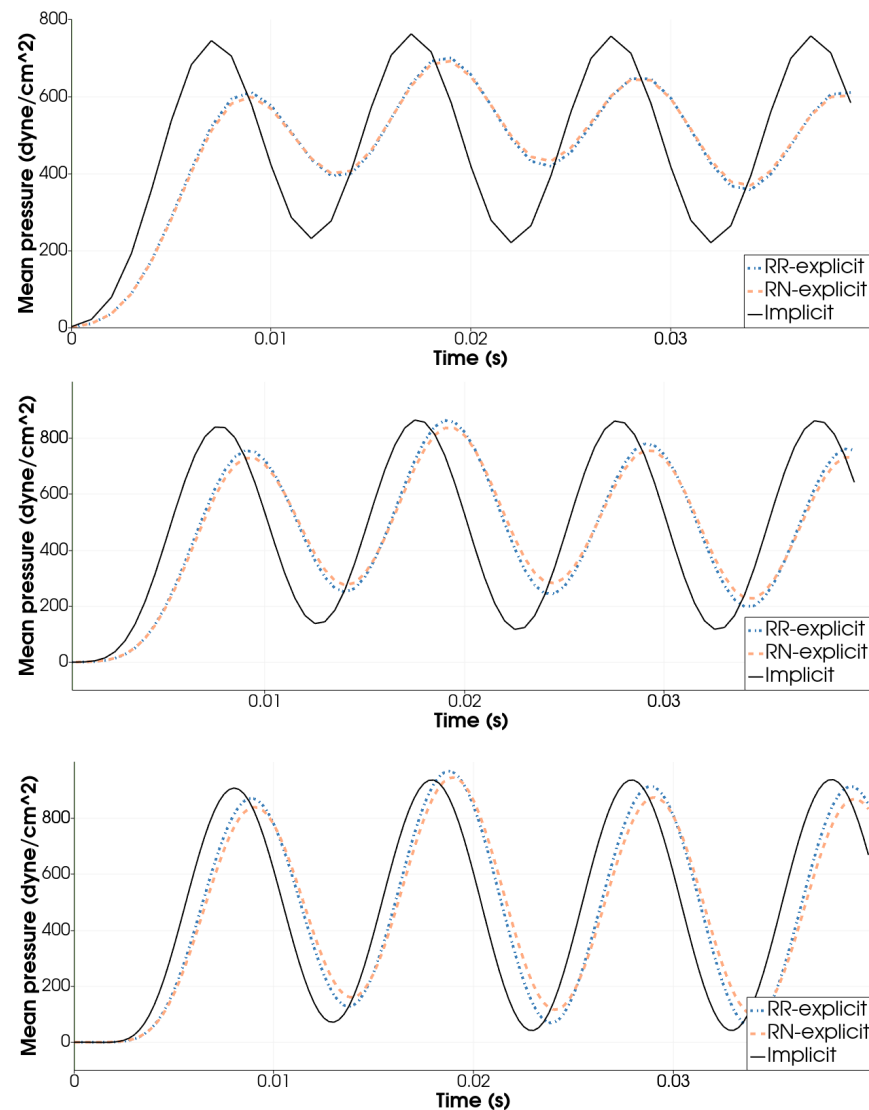
Figure 1. Mean pressure at section $z = 2.5\,\text{cm}$ for different values of Δt. Top: $\Delta t = 0.001$ s; Middle: $\Delta t = 0.0005$ s; Bottom: $\Delta t = 0.00025$ s. Test I.

From these results, we observe that the RR-Explicit and RN-Explicit solutions are in any case stable and feature a behavior which is reasonable if compared with the implicit solution, also depicted in the figures. As expected, decreasing Δt the two solutions tend to coincide with the implicit one, see Figures 1 and 2, top and middle. In addition, from Figure 2 we notice that the performances of the proposed explicit schemes seem to be robust with respect to the Reynolds number and the value of the surrounding tissue. In any case, the two explicit solutions seem to be very similar, thus the new strategy proposed in Section 3.3 to build an explicit RN scheme could be an effective way to obtain a loosely coupled scheme characterized by only one parameter.
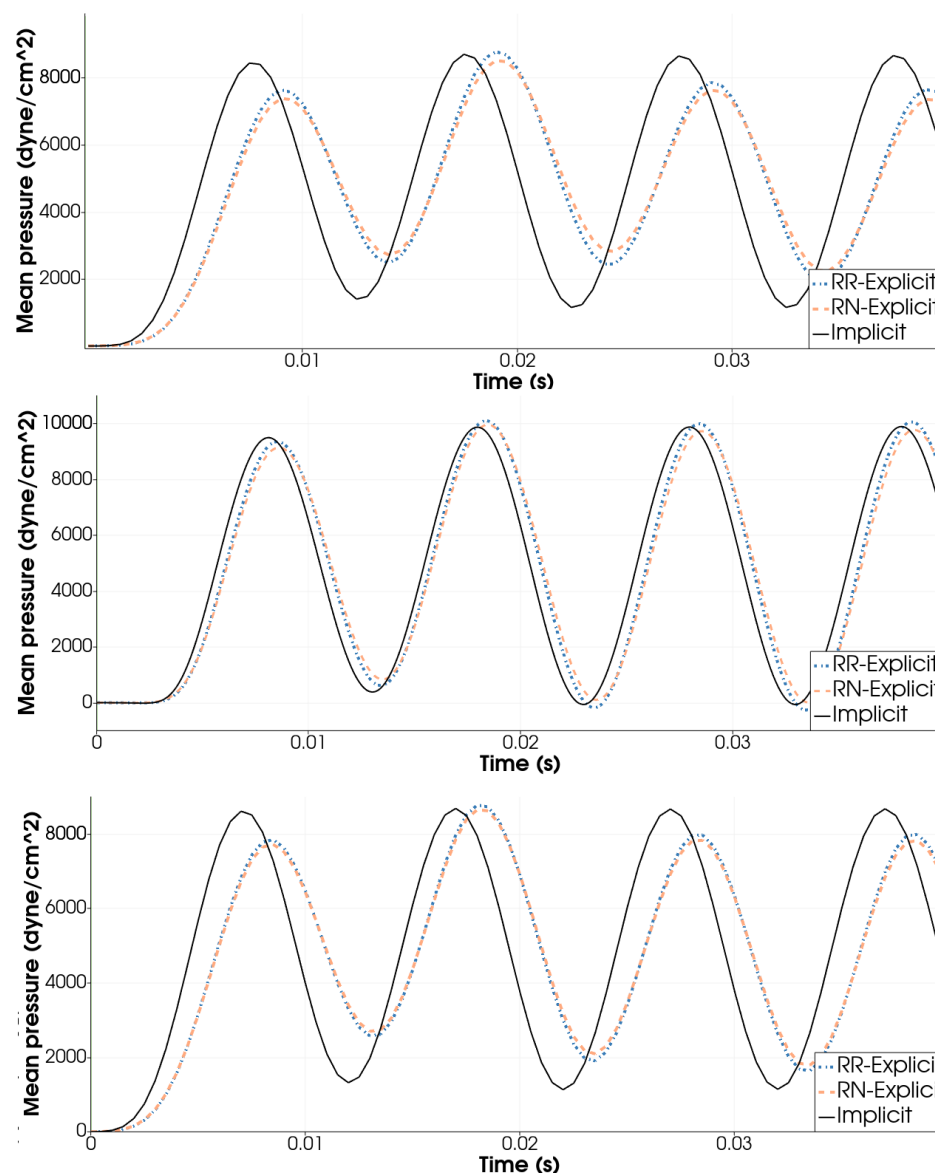
Figure 2. Mean pressure at section $z = 2.5$ cm for $\widehat{P} = 5000$: $\Delta t = 0.0005$ s, $\gamma_{ST} = 1.5 \times 10^5$ (**t**), $\Delta t = 0.000125$ s, $\gamma_{ST} = 1.5 \times 10^5$ (**middle**), and $\Delta t = 0.0005$ s, $\gamma_{ST} = 3 \times 10^5$ (**bottom**). Test I.

Remark 3. *Sometimes in the literature it is asserted that for FSI problems, among the solutions obtained with a strongly coupled (SC) scheme and with a loosely coupled (LC) scheme, the former is the reference one and the latter should be close to it to be considered accurate. However, we believe that a SC scheme features in general only better stability properties (being associated to an implicit time discretization) than a LC one (which is associated to an explicit time discretization). For values of Δt which guarantee stability of LC schemes, the accuracy of SC and LC methods is the same if*

discretization methods of the same order have been used. For example, in our case both methods are first order in time. The fact that the explicit solution seems to be more diffusive than the implicit one for not enough small values of Δt (see Figure 1, top and middle) could be ascribed to the fact the our Robin based LC schemes could be seen as stabilized methods where α_f and α_s play the role of stabilization parameters, whose influence on the solution increases with Δt.

4.3. Test in a Human Aortic Abdominal Aneurysm—Test II

In the second test (test II), we consider a human aortic abdominal aneurysm (AAA) reconstructed from CT images. At the inlet we prescribed the physiological Neumann condition (13) with

$$P_{in} = \begin{cases} 53,320 \, \sin(5\pi t) \, \text{dyne/cm}^2 & t \leq 0.2 \, \text{s}, \\ 0 \, \text{dyne/cm}^2 & 0.2 \, \text{s} < t \leq 0.8, \end{cases}$$

with absorbing resistance conditions at the outlets. For the structure we imposed the Robin condition (1f) with $\gamma_{ST} = 3 \times 10^6$ dyne/cm^3 at the external surface, and fixed inlet and outlets. We set $\Delta t = 0.001$ s. We considered the explicit RN and RR scheme with parameters estimated as described in Sections 3.2 and 3.3, respectively, by using the radius of the aneurysm (1.9 cm) as representative value for R. Moreover, we have used $H = 0.17$ cm for the structure thickness. The fluid and structure meshes were formed by 153 k and 74 k tetraedra, respectively, leading to the following ranges for the frequencies: $k \in [0.3, 19.6]$ cm^{-1} and $m \in [0, 38]$. In particular, the optimized interface parameters found by our analyses were $\alpha_f = 2174$ g/(cm^2 s), $\alpha_s = -85$ g/(cm^2 s) for the explicit RR scheme and $\alpha_f = 2229$ g/(cm^2 s) for the explicit RN scheme.

In Figures 3–5 we report the pressure field, the fluid velocity magnitude, and the vessel displacement magnitude at $t = 0.05$ s and $t = 0.1$ s (the latter being the systolic peak) for the explicit RR and RN schemes, together with an implicit solution. From these results we can observe stability of the proposed explicit schemes, reached for a value of Δt which is commonly used in hemodynamic applications to guarantee accuracy. Moreover, we observe very similar results between the explicit and implicit solutions, much more similar than those reported in Figure 1, upper, for the same value of Δt. This is probably due to the lower frequency of the physiological input signal used in test II with respect to that used for test I. All these observations are very encouraging in view of using the proposed loosely coupled schemes for real hemodynamic applications, a field where the strong added mass effect made the use of loosely coupled schemes a very challenging issue.

4.4. Final Remarks

We have considered a loosely coupled (explicit) partitioned algorithm based on Robin interface conditions for the numerical solution of FSI problem in the presence of large added mass effect. In particular, we focused on the selection of the interface parameters in the coupling conditions, which plays a crucial role in the stability of the method. The novelty of the paper relies on the description of an effective way to select the parameters in the interface conditions. This choice is crucial to improve stability of the proposed schemes, which, in general, is very poor when added mass effect is large. All the reported results (obtained in the hemodynamic regime when the added mass effect is very large) showed the stability of the numerical solution obtained by using the interface parameters proposed in this work.

The interest in using a partitioned scheme relies in its modularity, i.e., in the fact that we can use pre-existing separate fluid and structure codes and no ad-hoc implementation of a FSI solver is needed. Moreover, regarding the choice of an explicit/loosely coupled method, this is very attractive since, if stable, it allows for the reduction of computational costs with respect to implicit/fully coupled methods, if the need of using a smaller time step is compensated by the reduction of number of the subproblems we have to solve for each time step. In [29] we show for a test case that the CPU time of the explicit RN scheme was reduced by about three times with respect to the implicit RN case.
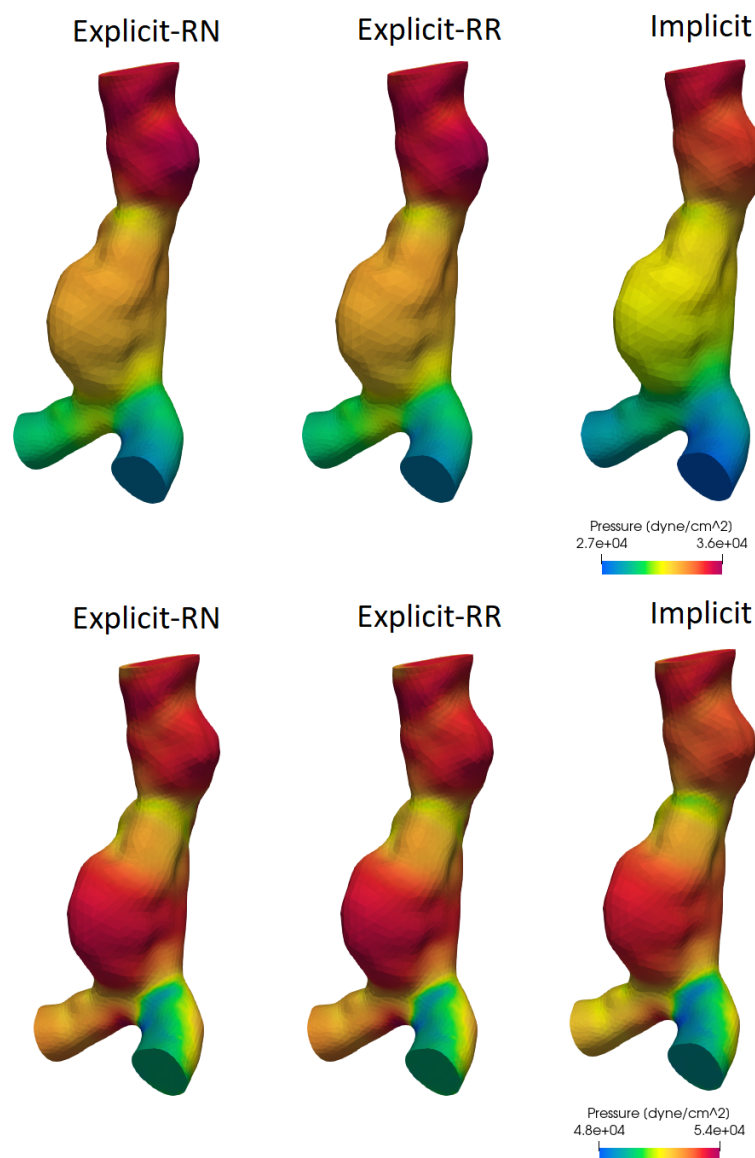
Figure 3. Pressure field for the AAA simulation. Top: $t = 0.05$ s; Bottom: $t = 0.1$ s. Test II.

Regarding the validation of our results, we observe that the results obtained by the library LifeV have been compared with analytical solutions and with clinical or experimental data. For the fluid solution, CFD results in the context of hemodynamics were successfully compared with experimental results in [43], with ECD measures in [44] and with PC-MRI data in [45]. Regarding FSI studies, in [41] the authors validated the numerical solution of implicit RR methods by comparing the results with an analytical solution.

Regarding test II in a human AAA, it provides the first results obtained with the proposed loosely coupled schemes in a real geometry in the context of hemodynamics and using data all in the hemodynamic regime. The results are stable and very similar to the implicit ones and highlight the ability of the method of representing the wave propagation and the deformation of the domains.
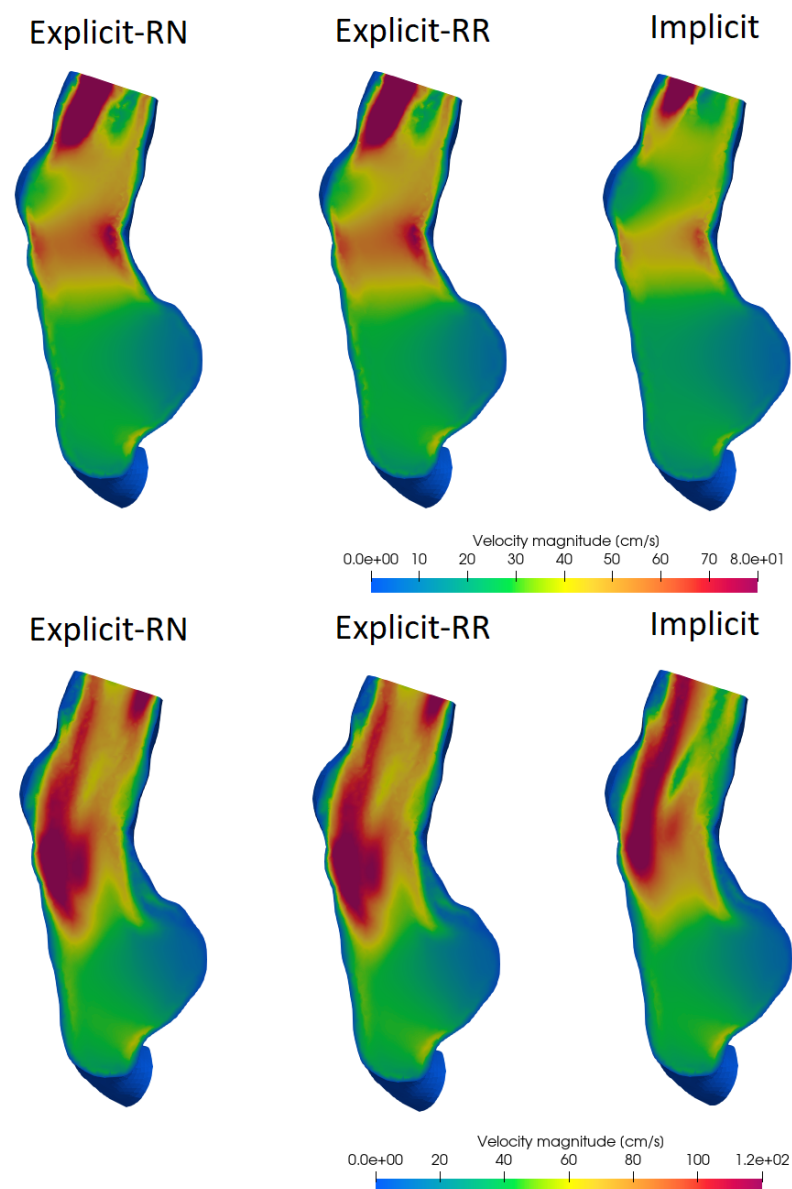
Figure 4. Velocity magnitude for the AAA simulation. Top: $t = 0.05$ s; Bottom: $t = 0.1$ s. Test II.

FSI results could provide important clinical indications about the evolution of a disease or the improvement of a therapy. We mention, for example, studies that quantified the stresses in carotid atherosclerotic plaques [46,47] or compared different surgical strategies for coronary bypasses [48,49]. However, often the application of FSI methods in such contexts has been limited due to the very high computational effort needed to numerically solve such problem. Our test in human AAA gives an important preliminary answer toward the use of explicit Robin–Robin and Robin–Neumann methods for clinical applications, with a dramatic savings in computational times with respect to strongly coupled (implicit) schemes.
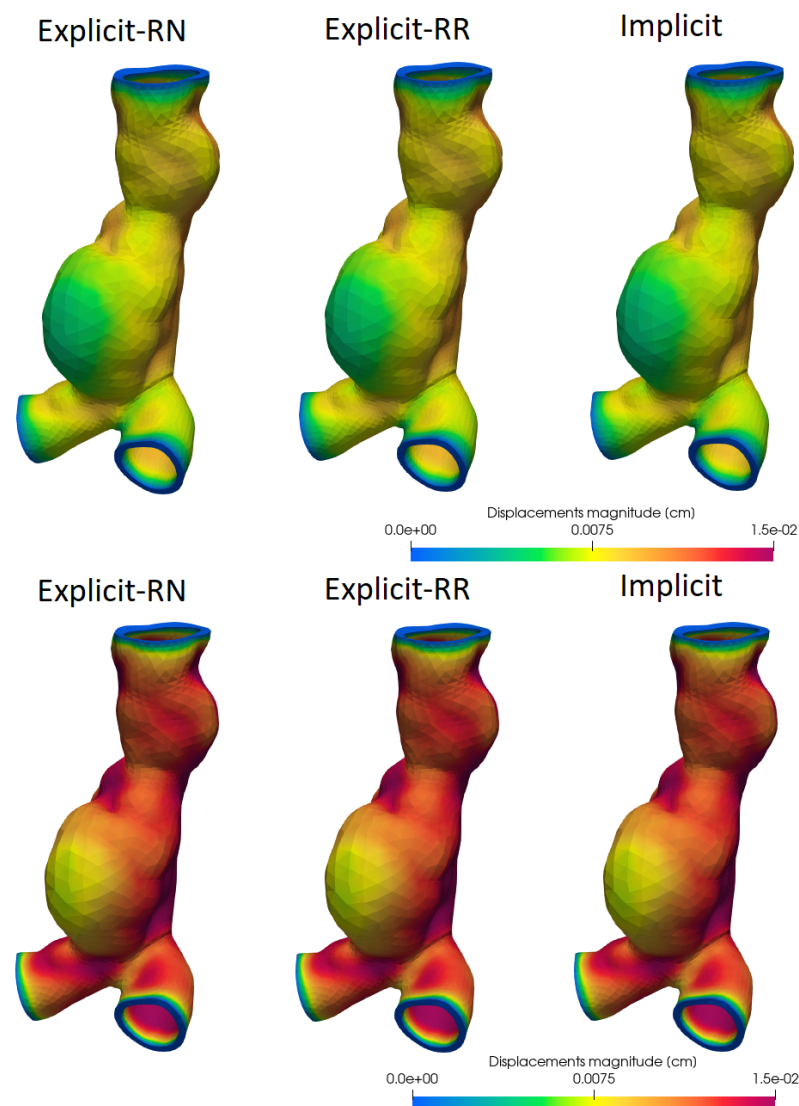
Figure 5. Displacements magnitude for the AAA simulation. Top: $t = 0.05$ s; Bottom: $t = 0.1$ s. Test II.

References

1. Heil, M. An efficient solver for the fully coupled solution of large-displacement fluid-structure interaction problems. *Comput. Methods Appl. Mech. Eng.* **2004**, *193*, 1–23. [CrossRef]
2. Crosetto, P.; Deparis, S.; Fourestey, G.; Quarteroni, A. Parallel Algorithms for Fluid-Structure Interaction Problems in Haemodynamics. *SIAM J. Sci. Comput.* **2011**, *33*, 1598–1622. [CrossRef]
3. Gee, M.; Kuttler, U.; Wall, W. Truly monolithic algebraic multigrid for fluid-structure interaction. *Int. J. Num. Methods Engrgy* **2011**, *85*, 987–1016. [CrossRef]
4. Barker, A.; Cai, X. Scalable parallel methods for monolithic coupling in fluid-structure interaction with application to blood flow modeling. *J. Comput. Phys.* **2010**, *229*, 642–659. [CrossRef]
5. Deparis, S.; Forti, D.; Grandperrin, G.; Quarteroni, A. FaCSI: A Block Parallel Preconditioner for Fluid-Structure Interaction in Hemodynamics. *J. Comput. Phys.* **2016**, *327*, 700–718. [CrossRef]
6. Bazilevs, Y.; Calo, V.; Hughes, T.; Zhang, Y. Isogeometric Fluid-Structure Interaction: Theory, algorithms, and computations. *Comput. Mech.* **2008**, *43*, 3–37. [CrossRef]
7. Causin, P.; Gerbeau, J.; Nobile, F. Added-mass effect in the design of partitioned algorithms for fluid-structure problems. *Comput. Methods Appl. Mech. Eng.* **2005**, *194*, 4506–4527. [CrossRef]
8. Kuttler, U.; Wall, W. Fixed-point fluid-structure interaction solvers with dynamic relaxation. *Comp. Mech* **2008**, *43*, 61–72. [CrossRef]
9. Badia, S.; Nobile, F.; Vergara, C. Fluid-structure partitioned procedures based on Robin transmission conditions. *J. Comput. Phys.* **2008**, *227*, 7027–7051. [CrossRef]
10. Badia, S.; Nobile, F.; Vergara, C. Robin-Robin preconditioned Krylov methods for fluid-structure interaction problems. *Comput. Methods Appl. Mech. Eng.* **2009**, *198*, 2768–2784. [CrossRef]
11. Nobile, F.; Vergara, C. Partitioned algorithms for fluid-structure interaction problems in haemodynamics. *Milan J. Math.* **2012**, *80*, 443–467. [CrossRef]
12. Nobile, F.; Pozzoli, M.; Vergara, C. Inexact accurate partitioned algorithms for fluid-structure interaction problems with finite elasticity in haemodynamics. *J. Comput. Phys.* **2014**, *273*, 598–617. [CrossRef]
13. Guidoboni, G.; Glowinski, R.; Cavallini, N.; Canic, S. Stable loosely-coupled-type algorithm for fluid–structure interaction in blood flow. *J. Comput. Phys.* **2009**, *228*, 6916–6937. [CrossRef]
14. Fernández, M.; Gerbeau, J.; Grandmont, C. A projection semi-implicit scheme for the coupling of an elastic structure with an incompressible fluid. *Int. J. Num. Methods Engrgy* **2007**, *69*, 794–821. [CrossRef]
15. Fernández, M. Incremental displacement-correction schemes for incompressible fluid-structure interaction - Stability and convergence analysis. *Numer. Math.* **2013**, *123*, 21–65. [CrossRef]
16. Dettmer, W.; Lovric, A.; Kadapa, C.; Peric, D. New iterative and staggered solution schemes for incompressible fluid-structure interaction based on Dirichlet-Neumann coupling. *Int. J. Num. Methods Engrgy* **2020**, 1–32. [CrossRef]
17. Park, K.; Felippa, C.; Runtz, J.D. Stabilisation of staggered solution procedures for fluid-structure interaction analysis. *Comput. Methods Appl. Mech. Eng.* **1977**, *26*.
18. Piperno, S.; Farhat, C. Partitioned prodecures for the transient solution of coupled aeroelastic problems-Part II: Energy transfer analysis and three-dimensional applications. *Comput. Methods Appl. Mech. Eng.* **2001**, *190*, 3147–3170. [CrossRef]
19. Farhat, C.; van der Zee, K.; Geuzaine, P. Provably second-order time-accurate loosely-coupled solution algorithms for transient nonlinear computational aeroelasticity. *Comput. Methods Appl. Mech. Eng.* **2006**, *195*, 1973–2001. [CrossRef]
20. Quarteroni, A.; Manzoni, A.; Vergara, C. The cardiovascular system: Mathematical modelling, numerical algorithms and clinical applications. *Acta Numer.* **2017**, *26*, 365–590. [CrossRef]
21. Forster, C.; Wall, W.; Ramm, E. Artificial added mass instabilities in sequential staggered coupling of nonlinear structures and incompressible viscous flow. *Comput. Methods Appl. Mech. Eng.* **2007**, *196*, 1278–1293. [CrossRef]
22. Nobile, F.; Vergara, C. An effective fluid-structure interaction formulation for vascular dynamics by generalized Robin conditions. *SIAM J. Sci. Comput.* **2008**, *30*, 731–763. [CrossRef]
23. Fernandez, M.; Mullaert, J.; Vidrascu, M. Explicit Robin–Neumann schemes for the coupling of incompressible fluids with thin-walled structures. *Comput. Methods Appl. Mech. Eng.* **2013**, *267*, 566–593. [CrossRef]
24. Bukac, M.; Canic, S.; Glowinski, R.; Tambaca, J.; Quaini, A. Fluid–structure interaction in blood flow capturing non-zero longitudinal structure displacement. *J. Comput. Phys.* **2013**, *235*, 515–541. [CrossRef]
25. Bukac, M.; Canic, S.; Glowinski, R.; Muha, B.; Quaini, A. A modular, operator-splitting scheme for fluid–structure interaction problems with thick structures. *Int. J. Num. Meth. Fluids* **2014**, *74*, 577–604. [CrossRef]
26. Lukacova-Medvid'ova, M.; Rusnakova, G.; Hundertmark-Zauskova, A. Kinematic splitting algorithm for fluid–structure interaction in hemodynamics. *Comput. Methods Appl. Mech. Eng.* **2013**, *265*, 83–106. [CrossRef]
27. Banks, J.; Henshaw, W.; Schwendeman, D. An analysis of a new stable partitioned algorithm for FSI problems. Part I: Incompressible flow and elastic solids. *J. Comput. Phys.* **2014**, *269*, 108–137. [CrossRef]
28. Burman, E.; Fernández, M. Explicit strategies for incompressible fluid-structure interaction problems: Nitsche type mortaring versus Robin–Robin coupling. *Int. J. Num. Methods Engrgy* **2014**, *97*, 739–758. [CrossRef]
29. Gigante, G.; Vergara, C. On the stability of a loosely-coupled scheme based on a Robin interface condition for fluid-structure interaction. *Comput. Math. Appl.* **2021**, *96*, 109–119. [CrossRef]

30. Gander, M. Optimized Schwarz Methods. *SIAM J. Numer. Anal.* **2006**, *44*, 699–731. [CrossRef]
31. Gigante, G.; Vergara, C. Analysis and optimization of the generalized Schwarz method for elliptic problems with application to fluid-structure interaction. *Numer. Math.* **2015**, *131*, 369–404. [CrossRef]
32. Donea, J. An arbitrary Lagrangian-Eulerian finite element method for transient dynamic fluid-structure interaction. *Comput. Methods Appl. Mech. Eng.* **1982**, *33*, 689–723. [CrossRef]
33. Quarteroni, A.; Dede, L.; Manzoni, A.; Vergara, C. *Mathematical Modelling of the Human Cardiovascular System—Data, Numerical Approximation, Clinical Applications*; Cambridge University Press: Cambridge, UK, 2019.
34. Moireau, P.; Xiao, N.; Astorino, M.; Figueroa, C.A.; Chapelle, D.; Taylor, C.A.; Gerbeau, J. External tissue support and fluid–structure simulation in blood flows. *Biomech. Model. Mechanobiol.* **2012**, *11*, 1–18. [CrossRef] [PubMed]
35. Wall, W.; Wiechert, L.; Comerford, A.; Rausch, S. Towards a comprehensive computational model for the respiratory system. *Int. J. Numer. Methods Biomed. Eng.* **2010**, *26*, 807–827. [CrossRef]
36. Swim, E.; Seshaiyer, P. A nonconforming finite element method for fluid-structure interaction problems. *Comput. Methods Appl. Mech. Eng.* **2006**, *195*, 2088–2099. [CrossRef]
37. Badia, S.; Quaini, A.; Quarteroni, A. Splitting methods based on algebraic factorization for fluid-structure interaction. *SIAM J. Sci. Comput.* **2008**, *30*, 1778–1805. [CrossRef]
38. Lebedev, N. *Special Functions and Their Applications*; Courier Dover Publications: Mineola, NY, USA, 1972.
39. Gigante, G.; Sambataro, G.; Vergara, C. Optimized Schwarz methods for spherical interfaces with application to fluid-structure interaction. *SIAM J. Sci. Comput.* **2020**, *42*, A751–A770. [CrossRef]
40. Gerardo Giorda, L.; Nobile, F.; Vergara, C. Analysis and optimization of Robin-Robin partitioned procedures in fluid-structure interaction problems. *SIAM J. Numer. Anal.* **2010**, *48*, 2091–2116. [CrossRef]
41. Nobile, F.; Pozzoli, M.; Vergara, C. Time accurate partitioned algorithms for the solution of fluid-structure interaction problems in haemodynamics. *Comput. Fluids* **2013**, *86*, 470–482. [CrossRef]
42. LifeV User Manual. 2010. Available online: http://lifev.org (accessed on 15 February 2021).
43. Passerini, T.; Quaini, A.; Villa, U.; Veneziani, A.; Canic, S. Validation of an open source framework for the simulation of blood flow in rigid and deformable vessels. *Int. J. Numer. Methods Biomed. Eng.* **2013**, *29*, 1192–1213. [CrossRef]
44. Guerciotti, B.; Vergara, C.; Azzimonti, L.; Forzenigo, L.; Buora, A.; Biondetti, P.; Domanin, M. Computational study of the fluid-dynamics in carotids before and after endarterectomy. *J. Biomech.* **2015**, *49*, 26–38. [CrossRef]
45. Faggiano, E.; Antiga, L.; Puppini, G.; Quarteroni, A.; Luciani, G.; Vergara, C. Helical flows and asymmetry of blood jet in dilated ascending aorta with normally functioning bicuspid valve. *Biomech. Model. Mechanobiol.* **2013**, *12*, 801–813. [CrossRef]
46. Gao, H.; Long, Q.; Graves, M.; Gillard, J.; Li, Z. Carotid arterial plaque stress analysis using fluid–structure interactive simulation based on in-vivo magnetic resonance images of four patients. *J. Biomech.* **2009**, *42*, 1416–1423. [CrossRef] [PubMed]
47. Bennati, L.; Vergara, C.; Domanin, M.; Malloggi, C.; Bissacco, D.; Trimarchi, S.; Silani, V.; Parati, G.; Casana, R. A computational fluid structure interaction study for carotids with different atherosclerotic plaques. *J. Biomech. Eng.* **2021**, in press. [CrossRef] [PubMed]
48. Kabinejadian, F.; Ghista, D. Compliant model of a coupled sequential coronary arterial bypass graft: Effects of vessel wall elasticity and non-Newtonian rheology on blood flow regime and hemodynamic parameters distribution. *Med. Eng. Phys.* **2012**, *34*, 860–872. [CrossRef] [PubMed]
49. Guerciotti, B.; Vergara, C.; Ippolito, S.; Quarteroni, A.; Antona, C.; Scrofani, R. A computational fluid-structure interaction analysis of coronary Y-grafts. *Med. Eng. Phys.* **2017**, *47*, 117–127. [CrossRef] [PubMed]